Laboratory Rotational Spectrum of PH ($N = 2 \leftarrow 1$) in the 1 THz Region

E. Klisch, H. Klein, G. Winnewisser, and E. Herbst[a]

I. Physikalisches Institut, Universität zu Köln, D-50937 Köln

[a] Departments of Physics and Astronomy, The Ohio State University, Columbus, OH 43210, USA

Z. Naturforsch. **53 a,** 733–742 (1998); received July 8, 1998

The $N = 2 \leftarrow 1$ rotational transition of the PH radical in its ground electronic ($X^3\Sigma^-$) and vibrational states has been measured with the Cologne terahertz spectrometer in the frequency region between 920 and 1070 GHz. The PH radical was generated by immersing red phosphorus in a dc glow discharge of molecular hydrogen buffered with argon. Transition frequencies of the five $J' - J''$ fine structure components together with the associated hyperfine structure patterns were precisely measured and analyzed to derive highly accurate molecular parameters, which are more extensive than those reported in the existing literature. Among the determined parameters are the rotational constant $B_0 = 252200.8099(63)$ MHz and the centrifugal distortion constant $D_0 = 13.2915(33)$ MHz, as well as two fine structure constants – the spin-rotation constant γ_0 and the spin-spin interaction constant λ_0 – together with their centrifugal distortion contributions D_{γ_0} and D_{λ_0}. Furthermore, each of the magnetic hyperfine parameters b_F, c, and the nuclear spin-rotation constants C_I were obtained for both nuclei. The accuracy of previously obtained molecular constants has been improved by up to one order of magnitude. This new set of molecular parameters allows highly reliable frequency predictions of the rotational spectrum extending into the far infrared region; such transition frequencies may be of interest for interstellar spectroscopy.

I. Introduction

Since the successful introduction of broad-band spectroscopy in the terahertz region at Cologne University [1], it has been one of the major scientific pursuits of our laboratory to measure the rotational spectra of light hydrides with high resolution and with high accuracy. Among these light hydrides, the diatomic radicals assume a special role, both spectroscopically and astrophysically. Spectroscopically, the analysis of highly precise measurements reveals further insight into the coupling schemes of various angular momenta arising from the interaction between the rotational and the electronic motions of the molecular radical, known as Hund's coupling cases (a) - (e) [2]. Astrophysically, the diatomic hydrides occur as important intermediates in chemical reaction networks in interstellar clouds.

With high resolution broad-band spectroscopy in the terahertz region, we have previously studied among many other radicals the diatomic ones SH, SD [3, 4], NH [5] and ND [6]. Here we turn our attention to PH, a fundamental species with spectral properties that have been studied in the laboratory in different regions of the electromagnetic spectrum. The electronic spectrum of the PH radical has long been studied and analyzed, and molecular parameters have been derived (see e. g. [7]). For example, the analysis of the rotational structure of the $A^3\Pi_i - X^3\Sigma^-$ band system of PH and PD [8] yielded molecular constants for the two electronic states of both molecules.

The investigation of the pure rotational spectrum of PH was started in 1975 by Davies *et al.* [9] with the detection of the $N = 5 \leftarrow 4$ rotational transition in both the electronic ground state and the $a^1\Delta$ excited state. The technique employed was laser magnetic resonance spectroscopy (LMR). Uehara and Hakuta [10] subsequently extended these observations to the ro-vibrational transitions $v = 1 \leftarrow 0$ of PD using a CO laser LMR spectrometer. With far-infrared LMR techniques, using six different laser lines between 570.6 and 164.6 μm as radiation sources, Ohashi *et al.* [11] recorded a variety of low N rotational lines of PH and PD, and obtained molecular parameters for the two species. The resolution of their spectra was high enough to resolve the magnetic hyperfine splitting of the ^{31}P ($I = 1/2$) nucleus for the $v = 0$ and for the $v = 1$ state of PD, and, consequently, the hyperfine coupling

Reprint requests to Prof. G. Winnewisser; Fax: +49 221 470 5162, E-mail: winnewisser@ph1.uni-koeln.de.

0932–0784 / 98 / 0900–0733 $ 06.00

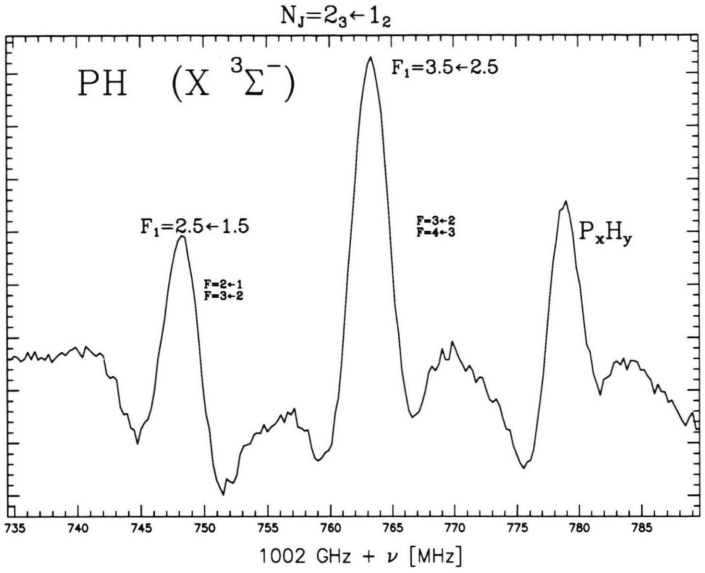

Fig. 1. Recorded spectrum of the $N, J = 2,3 \leftarrow 1,2$ rotational-fine structure transition of PH near 1 THz. The hyperfine splitting due to the contribution of the hydrogen nucleus is resolved. Although the inclusion of the phosphorus nucleus yields an additional doublet splitting, this is not resolved within the Doppler limit of our spectrometer. The line at 1002780 MHz is not identified, but is expected to arise from a more complex hydride P_xH_y ($x, y = 1, 2, \ldots$) which is simultaneously generated in the discharge cell.

constants pertaining to this nucleus were determined. For PH the magnetic splitting of the ^{1}H ($I = 1/2$) nucleus could be resolved as well.

Goto and Saito [12] were the first to use millimeter-wave techniques to measure the lowest rotational transitions of the PH and PD radicals. They employed a source-modulated solid state oscillator with subsequent frequency multipliers to send radiation through a glow-discharge free-space absorption cell. For PH, a total of twenty fine and hyperfine components of the $N = 1 \leftarrow 0$ transition between 423 and 554 GHz were measured, whereas for PD two rotational transitions were studied – $N = 1 \leftarrow 0$ and $N = 2 \leftarrow 1$ – with a total of 50 different components. For all three nuclei, P, H, and D, the magnetic hyperfine parameters were determined from a least-squares fitting to the observed spectral lines.

In addition to its spectroscopic significance, PH may be detectable in interstellar clouds. Two phosphorus bearing molecules, PN and CP, have been detected in the interstellar medium [13, 14], but the important phosphorus hydrides, PH, PH_2, and PH_3 remain so far unidentified, although their rotational spectra are now known to a reasonable degree of accuracy. One reason for their non-detection is that most of their rotational transitions fall into frequency regions with strongly reduced atmospheric transmission, and these frequencies are therefore difficult to observe from ground-based observatories. For example, the $N = 1 \leftarrow 0$ and $N = 2 \leftarrow 1$ transitions of PH fall in the 423 to 554 GHz and 920 to 1070 GHz regions, respectively. The lower frequency transition occurs in a region of significant atmospheric interference; the transmission around 490 GHz is only 40 %. For the upper frequency transition, the atmosphere is essentially opaque. Airborne and satellite measurements would be useful to detect the phosphorus hydrides in interstellar space.

It is the purpose of the present paper to report extended frequency measurements of the $N = 2 \leftarrow 1$ rotational transition of PH carried out with the Cologne terahertz spectrometer. Together with the precise measurements of Goto andSaito [12], these new data yield a complete set of highly accurate molecular parameters from which very reliable frequency predictions result for the higher rotational transitions. These results are of interest for interstellar observations, so we discuss estimates of the interstellar abundance of PH.

II. Experimental

As the source of radiation, we used a backward wave oscillator (BWO) with a frequency range of 874 - 1100 GHz supplied by the ISTOK Research and Production Company (Fryazino, near Moscow). The BWO was frequency stabilized by phase-locking its output to a local oscillator (KVARZ synthesizer), which uses a 5 MHz signal from a rubidium frequency standard as external reference. The absorption signal was detected with a liquid helium cooled,

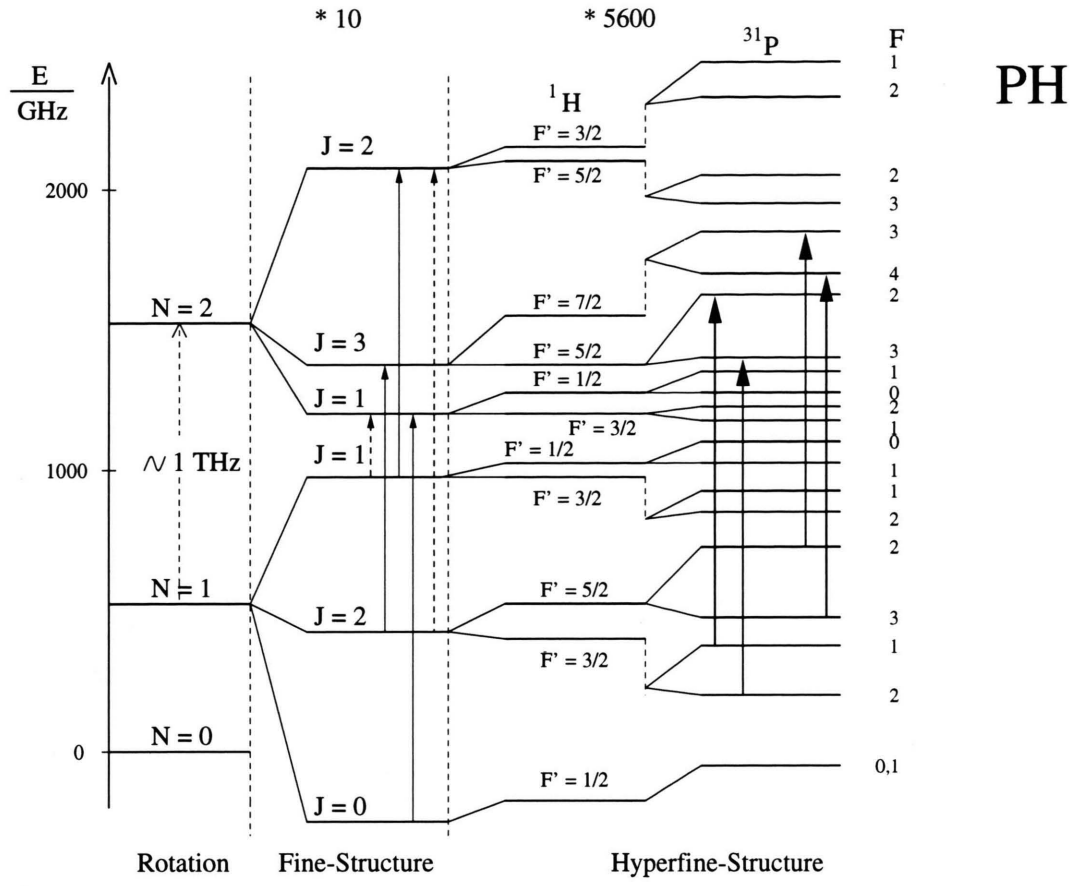

Fig. 2. Section of the energy level diagram of PH ($^3\Sigma^-$). The fine structure terms are enlarged 10 times. Bold arrows mark observed transitions with higher intensity ($\Delta J = 1$), dotted arrows mark observed transitions with lower intensity ($\Delta J = 0$). The hyperfine structure contributions of ^{1}H and ^{31}P are enlarged 5600 times. Both recorded transitions in Fig. 1 ($F_1 = 2.5 \leftarrow 1.5$ and $F_1 = 3.5 \leftarrow 2.5$) are split further by the phosphorus nucleus into neighboring doublets, which experimentally are not observed. Here we emphasize that this interpretation of the observed splitting depends on the order of the coupling scheme of the nuclear spins as noted in the text. The observed splitting thus could equally well be interpreted as caused by the phosphorus nucleus.

magnetically tuned InSb hot-electron bolometer. Further details of the terahertz spectrometer are described by Winnewisser [1] and Belov *et al.* [15]. The PH radical was produced in a dc discharge of hydrogen over red phosphorus. The optimum PH production parameters are 150 μbar pressure of hydrogen and a discharge current of 310 mA. In addition to PH spectral transitions, many additional lines are caused by a carrier or carriers with the chemical formula P_xH_y. The lines appear in second derivative form because of the 2ν frequency modulation. The accuracy of most lines is estimated to range between 10 and 100 kHz. The quoted uncertainties for the measured transition frequencies reflect the partially unresolved hyperfine structure and not the experimental uncertainties, which for unblended lines are below 10 kHz. In the case of unstable species, which are produced in a dc discharge, the experimental uncertainty for resolved lines is about 50 - 100 kHz.

Figure 1 depicts a section of the $N, J = 2, 3 \leftarrow 1, 2$ rotational-fine structure transition recorded near 1 THz. For this transition, the hyperfine structure is characterized by two hyperfine doublets with differing quantum numbers $F_1 + 1 \leftarrow F_1$; the angular momentum $\boldsymbol{F}_1$ arises from the coupling between $\boldsymbol{J}$ and the spin $\boldsymbol{I}_1$ of the hydrogen nucleus, ^{1}H. An additional splitting caused by the further coupling of $\boldsymbol{F}_1$ with the spin $\boldsymbol{I}$ of the phosphorus nucleus, ^{31}P, produces differ-

ing values of the total quantum number F. Since the latter coupling effect is weaker, the splitting could not be resolved yet. An energy level diagram focusing on the $N = 2 \leftarrow 1$ transition is depicted in Figure 2.

III. Theory and Analysis

The electronic ground state of PH is of $^3\Sigma^-$ symmetry, leading to a splitting of the rotational levels by fine structure effects. The Hamiltonian, H, describing the PH rotational-fine structure-hyperfine structure energy levels in the ground electronic state consists of three parts:

$$H = H_{\text{rot}} + H_{\text{fs}} + H_{\text{hfs}}, \tag{1}$$

where the subscripts "rot", "fs", and" hfs" refer to the rigid-body rotation, the fine structure, and the hyperfine structure contributions, respectively. The fine structure is caused by the spin-rotation interaction, characterized by the parameter γ, and the spin-spin interaction, characterized by the parameter λ. The spin-spin interaction dominates; the parameter λ amounts to 26 % of the rigid-body rotational parameter B itself. In the case of PH, the spin-rotation interaction has a negative sign and thus actually decreases the fine structure splitting. The hyperfine contribution in (1) is determined by both the ^{31}P nucleus and the ^{1}H nucleus, and represents the magnetic dipole interactions; i. e, the Fermi contact and the dipole-dipole terms, as well as the interaction of the nuclear spins with the rigid-body rotation of the molecule.

The Hamiltonian is evaluated in an extension of the Hund's case ($b_{\beta J}$) representation (Townes and Schawlow [16]), in which the rigid-body angular momentum $\boldsymbol{N}$ and the electronic spin angular momentum $\boldsymbol{S}$ first couple together to form a resultant $\boldsymbol{J}$, which then couples with the nuclear spin angular momentum $\boldsymbol{I}_1$ of the hydrogen, ^{1}H, which possesses a nuclear magnetic dipole moment of 2.7928456 (1) nuclear magnetons (IUPAC [17]) to form $\boldsymbol{F}_1$. The nuclear spin $\boldsymbol{I}_1$ couples closely to the quantization axis. The phosphorus nucleus, with a smaller magnetic dipole moment of 1.13160 (1) magnetons (IUPAC [17]), shows weaker coupling between its spin $\boldsymbol{I}$ and the quantization axis. Consequently, one would expect a significantly greater splitting from the hydrogen nucleus than from the phosphorus nucleus. It should be noted that this is not obvious from the sizes of the hyperfine constants in Table 2. However, the magnetic hyperfine interactions b_{F}, defined by Frosch and Foley [18], result in a relation to both, the nuclear magnetic spin moment μ_{I} – here given in nuclear magnetons μ_{N} – and the probability for the electron to be located at the nucleus:

$$b_{\text{F}} = b + \frac{c}{3} = \frac{e^2\hbar}{3 \cdot 10^6 \pi m_{\text{e}} m_{\text{p}} c^2} \frac{\mu_{\text{I}}/\mu_{\text{N}}}{I} \mid \psi_{(0)} \mid^2 .$$

Thus the greater values for b_F and c of the phosphorus nucleus are due to a higher probability of the two electrons to be located at ^{31}P than at ^{1}H.

The complete coupling scheme is

$$\begin{aligned} \boldsymbol{J} &= \boldsymbol{N} + \boldsymbol{S}, \\ \boldsymbol{F}_1 &= \boldsymbol{J} + \boldsymbol{I}_1 \quad (^1\text{H}), \\ \boldsymbol{F} &= \boldsymbol{F}_1 + \boldsymbol{I} \quad (^{31}\text{P}). \end{aligned}$$

We draw the attention to the choice on the order of coupling of the nuclear spins of the hydrogen and the phosphorus nuclei. The general rule we followed here, is that the nuclear spin with the stronger magnetic dipole moment – here the hydrogen ($\boldsymbol{I}_1$) – is taken to form $\boldsymbol{F}_1$, whereas the nuclear spin with the smaller moment – here the phosphorus ($\boldsymbol{I}$) – is added to $\boldsymbol{F}_1$ in order to obtain $\boldsymbol{F}$. Goto and Saito [12] decided for the other coupling scheme, i. e. $\boldsymbol{F}_1 = \boldsymbol{J} + \boldsymbol{I}_1$ (^{31}P) and $\boldsymbol{F} = \boldsymbol{F}_1 + \boldsymbol{I}$ (^{1}H). The reason for their coupling scheme could be that in the case of PH the stronger hyperfine coupling is due to the significantly higher probability of the electron's spin density around the phosphorus than around the hydrogen nucleus. However, for molecules with almost the same electronegativity – phosphorus and hydrogen have about the same value of 2.1 – the identification of the two nuclear spins with $\boldsymbol{I}_1$ and $\boldsymbol{I}$ is by no means uniquely defined.

Since H_{rot} represents the largest of the three contributions, the energy levels are ordered according to the rotational quantum number N. The fine structure, arising predominantly from the two electron spins interacting with each other, leads to a triplet structure, with levels characterized by quantum numbers $J = N - 1$, $J = N$ and $J = N + 1$. The coupling of the electron spin with the rigid-body rotation yields a relatively small contribution to the fine structure. We use the same matrix elements for H in the Hund's case ($b_{\beta J}$) representation as described previously in Klisch et al. [19], whereby, in addition, H_{Hfs} here has to be extended for two nuclei:

$$\langle N'SJ'I_1IF_1F \mid \hat{H} \mid NSJI_1IF_1F\rangle =$$

$$\left\{[B - D\,N(N+1)]N(N+1) + (\gamma + D_\gamma N(N+1))\frac{1}{2}[J(J+1) - N(N+1) - S(S+1)]\right\}\delta_{N',N}\,\delta_{J',J}$$

$$+\frac{1}{2}\left\{\lambda + D_\lambda[N(N+1) + N'(N'+1)]\right\}\frac{2\sqrt{3}}{3}(-)^{N+J+1}\begin{Bmatrix} J & 1 & N' \\ 2 & N & 1 \end{Bmatrix}(-)^{N'}\sqrt{(2N+1)(2N'+1)}\begin{pmatrix} N' & 2 & N \\ 0 & 0 & 0 \end{pmatrix}\delta_{J',J}$$

$$+(-)^{I+J'+F}\sqrt{I(I+1)(2I+1)(2J+1)(2J'+1)}\begin{Bmatrix} F & J' & I \\ 1 & I & J \end{Bmatrix}$$

$$\times\left\{\sqrt{2(S+1)(2S+1)}\left[b_F\delta_{N',N}(-)^{S+N+J+1}\begin{Bmatrix} S & J' & N \\ J & S & 1 \end{Bmatrix} - c\frac{\sqrt{30}}{3} + (-)^{N'}\begin{Bmatrix} S & S & 1 \\ N' & N & 2 \\ J' & J & 1 \end{Bmatrix}\begin{pmatrix} N' & 2 & N \\ 0 & 0 & 0 \end{pmatrix}\right]\right.$$

$$\left. + C_{\mathrm{I}}\,\delta_{N',N}\sqrt{N(N+1)(2N+1)}(-)^{S+N+J'+1}\begin{Bmatrix} N & J' & S \\ J & N & 1 \end{Bmatrix}\right\}$$

$$+(-)^{I_1+2F_1'+F+I_1+J}\begin{Bmatrix} F & F_1' & I_1 \\ 1 & I_1 & F_1 \end{Bmatrix}\sqrt{I_1(I_1+1)(2I_1+1)(2J+1)(2J'+1)(2F_1+1)(2F_1'+1)}\begin{Bmatrix} J' & F_1' & I_1 \\ F_1 & J & 1 \end{Bmatrix}$$

$$\times\left\{\sqrt{S(S+1)(2S+1)}\left[b_F^{(1)}\,\delta_{N',N}(-)^{S+N+J+1}\begin{Bmatrix} S & J' & N \\ J & S & 1 \end{Bmatrix} - c^{(1)}\frac{\sqrt{30}}{3}(-)^{N'}\begin{Bmatrix} S & S & 1 \\ N' & N & 2 \\ J' & J & 1 \end{Bmatrix}\begin{pmatrix} N' & 2 & N \\ 0 & 0 & 0 \end{pmatrix}\right]\right.$$

$$\left. + C_{\mathrm{I}}^{(1)}\,\delta_{N',N}\sqrt{N(N+1)(2N+1)}\begin{Bmatrix} N & J' & S \\ J & N & 1 \end{Bmatrix}\right\}.$$

The spectral lines have been assigned and fitted to the Hamiltonian by a non-linear least squares procedure. In the fitting procedure, the observed frequencies were weighted proportionally to the inverse square of their experimental uncertainties. The frequencies of the unresolved hyperfine splittings were calculated as the weighted average of the individual hyperfine components due to their relative intensities.The observed frequencies ν are listed in Table 1 along with quantum numbers J, F_1, F, residuals (observed – calculated frequencies), lower state energies (cm^{-1}), and Einstein-A-coefficients (s^{-1}), which are obtained from the formula

$$A_{m\to n} = \frac{64\pi^4\nu_{mn}^3}{3hc^3}\mu^2(2N+1)(2N'+1)\begin{pmatrix} N' & 1 & N \\ 0 & 0 & 0 \end{pmatrix}^2(2J'+1)\begin{Bmatrix} N' & J' & S \\ J & N & 1 \end{Bmatrix}^2$$

$$\times(2F_1'+1)(2F_1+1)\begin{Bmatrix} J' & F_1' & I_1 \\ F_1 & J & 1 \end{Bmatrix}^2(2F'+1)(2F+1)\begin{Bmatrix} F_1' & F' & I \\ F & F_1 & 1 \end{Bmatrix}^2.$$

To the best of our knowledge, the permanent electric dipole moment μ of PH has not been measured. To obtain a value for μ, we used the GAUSSIAN 94 program [20]. At the MP4/6-311G**-level of theory (fourth-order Moller-Plesset perturbation theory) with the experimentally obtained average bond distance $\langle r\rangle$ = 1.43283 Å, the program yields the value μ = 0.631 Debye. This value of the dipole moment has been used in the formula for the Einstein-A-coefficients.

The molecular parameters obtained from a global fitting procedure to our data and the lower frequency data of Goto and Saito [12] are listed in Table 2. Inclusion of the newly measured $N = 2 \leftarrow 1$ rotational transition required additional centrifugal correction terms characterized by the parameters D for the rotation, D_λ for the spin-spin interaction, and D_γ for the spin-rotation interaction. The obtained rotational parameter B_0 is in good agreement with the value of Goto and Saito [12], while the magnetic hyperfine parameters have been improved in precision by one order of magnitude. It should be noted that the different order of the coupling of

J'	F'_1	F'	$\leftarrow$	J''	F''_1	F''	ν/[MHz][a]	Res./[MHz]	E''/[cm^{-1}]	A/[s^{-1}]
1	1.5	1		1	1.5	1	927 174.343 (200)	− 0.162	18.466	0.000 113
1	1.5	2		1	1.5	2	927 236.690 (250)	− 0.179	18.465	0.000 202
1	0.5	1		1	0.5	1	927 433.779 (150)	+ 0.082	18.470	0.000 070
3	2.5	2		2	2.5	2	1 002 504.822 (150)[b]	+ 0.277	16.493	0.000 067
3	2.5	3		2	2.5	3			16.491	0.000 083
3	2.5	2		2	1.5	1	1 002 748.231 (50)[b]	+ 0.002	16.483	0.001 280
3	2.5	3		2	1.5	2			16.483	0.001 280
3	3.5	3		2	2.5	2	1 002 763.289 (200)[b]	+ 0.298	16.493	0.001 296
3	3.5	4		2	2.5	3			16.493	0.001 296
3	3.5	4		2	2.5	3			16.491	0.001 756
3	2.5	2		2	1.5	2	1 002 805.609 (250)	− 0.195	16.483	0.000 085
3	3.5	3		2	2.5	2	1 002 821.275 (250)	+ 0.047	16.491	0.000 069
2	1.5	1		1	0.5	1	1 008 320.074 (150)	+ 0.003	18.470	0.000 249
2	1.5	2		1	0.5	1	1 008 328.592 (100)	− 0.056	18.470	0.000 610
2	1.5	1		1	0.5	1	1 008 342.533 (100)	+ 0.187	18.470	0.000 135
2	2.5	2		1	1.5	1	1 008 386.931 (100)	− 0.067	18.466	0.000 679
2	2.5	3		1	1.5	2	1 008 395.416 (100)	− 0.084	18.465	0.001 044
2	2.5	2		1	1.5	2	1 008 408.154 (250)	− 0.324	18.465	0.000 067
2	1.5	1		1	1.5	1	1 008 466.109 (250)	+ 0.208	18.466	0.000 052
2	1.5	2		1	1.5	2	1 008 474.048 (100)	− 0.063	18.465	0.000 120
1	1.5	1		0	0.5	1	1 057 347.941 (100)[b]	+ 0.043	14.123	0.000 159
1	1.5	1		0	0.5	0			14.123	0.000 262
1	1.5	2		0	0.5	1	1 057 388.131 (100)	− 0.047	14.123	0.000 691
1	0.5	0		0	0.5	1	1 057 689.794 (250)	− 0.032	14.123	0.000 138
1	0.5	1		0	0.5	1	1 057 730.375 (100)[b]	+ 0.018	14.123	0.000 262
1	0.5	1		0	0.5	0			14.123	0.000 153
2	2.5	2		2	2.5	2	1 067 515.491 (100)	− 0.049	16.493	0.000 264
2	2.5	3		2	2.5	3	1 067 561.861 (100)	+ 0.046	16.491	0.000 380
2	1.5	1		2	1.5	1	1 067 836.897 (200)	− 0.182	16.485	0.000 138
2	1.5	2		2	1.5	2	1 067 883.703 (150)	+ 0.150	16.483	0.000 246

Table 1. Observed hyperfine components of PH in its $N = 2 \leftarrow 1$ rotational transition.

[a] Numbers in parentheses denote the estimated uncertainties of measured frequencies in units of the last quoted digit.
[b] Unresolved transition due to the two hfs-components being located within the Doppler width of around 1.4 MHz.

Table 2. Electronic ground-state rotational parameters[a] of PH.

Parameter		This work	Goto and Saito
B_0		252 200.809 9 (63)	252 200.827 8 (70)
D_0		13.291 5 (33)	13.301[b]
λ_0		66 255.564 (43)	66 255.701 (18)
D_{λ_0}		0.064 (20)	—
γ_0		–2 305.523 (15)	–2305.584 (12)
D_{γ_0}		0.364 (10)	0.392[b]
b_F	(H)	–46.542 8 (40)	–46.545 (19)
c	(H)	19.386 (56)	19.41 (14)
C_I	(H)	–0.037 8 (16)	–0.036 (28)
b_F	(P)	128.111 9 (42)	128.119 (17)
c	(P)	–476.836 (26)	–476.843 (78)
C_I	(P)	0.613 (54)	0.614 (27)

[a] Molecular parameters are given in MHz. Numbers in parentheses denote the standard deviation in units of the last quoted digit.
[b] Fixed.

the nuclear spins between Goto and Saito [12] and the present *Paper* does not affect the molecular parameters at all. The numbers in parentheses in Table 2 denote 1σ uncertainties in units of the last digit before the parentheses. The 1 THz spectroscopy proves to be suited for hyperfine interaction of PH due to ^{31}P since for lower rotational states the splitting is rough about the same order of the ^{1}H. This is in connection with the electronegativity of the two atoms (≈ 2.1), which is almost identical. Only for higher rotational states, the different matrix elements for the two nuclear spins cause a rather uncoupling of $\mathbf{I}$ than for $\mathbf{I}_1$ because of the smaller nuclear magnetic moment μ_I. This effect leads to a stronger collapse for the hyperfine components of the phosphorus than of the hydrogen atom. Therefore splittings caused by ^{31}P are difficult to observe in the IR region.

Predicted transition frequencies for unmeasured transitions along with Einstein-A-coefficients are of possible interest for astrophysicists. In Table 3, we use the parameters in Table 2 to predict a variety of transition frequencies for PH ranging upwards from 1.44 to 5.96 THz. In addition to the transition frequencies, we list associated quantum numbers, Einstein-A-coefficients, and lower state energies. Four quantum numbers (N, J, F_1, F) are listed for upper

Table 3. Predicted rotational transition (N' J' F_1' F' ← N'' J'' F_1'' F'') frequencies of PH.

N'	J'	F_1'	F'	N''	J''	F_1''	F''	ν [MHz][a,b]	A [s^{-1}]	E'' [cm^{-1}]
3.0	2.0	2.5	2.0	2.0	2.0	1.5	1.0	1 440 633.74	1.889E-05	52.104
3.0	2.0	2.5	3.0	2.0	2.0	1.5	2.0	1 440 692.95	2.957E-05	52.104
3.0	2.0	2.5	2.0	2.0	2.0	2.5	2.0	1 440 712.37	2.582E-04	52.102
3.0	2.0	2.5	2.0	2.0	2.0	2.5	3.0	1 440 725.79	1.963E-05	52.101
3.0	2.0	2.5	3.0	2.0	2.0	2.5	2.0	1 440 758.12	1.660E-05	52.102
3.0	2.0	2.5	3.0	2.0	2.0	2.5	3.0	1 440 771.54	3.701E-04	52.101
3.0	2.0	1.5	1.0	2.0	2.0	1.5	1.0	1 440 953.49	1.341E-04	52.104
3.0	2.0	1.5	1.0	2.0	2.0	1.5	2.0	1 440 966.95	2.865E-05	52.104
3.0	2.0	1.5	2.0	2.0	2.0	1.5	1.0	1 440 999.22	2.572E-05	52.104
3.0	2.0	1.5	2.0	2.0	2.0	1.5	2.0	1 441 012.67	2.400E-04	52.104
3.0	2.0	1.5	1.0	2.0	2.0	2.5	2.0	1 441 032.12	1.603E-05	52.102
3.0	2.0	1.5	2.0	2.0	2.0	2.5	3.0	1 441 091.26	2.664E-05	52.101
3.0	2.0	2.5	2.0	2.0	3.0	3.5	3.0	1 505 466.38	1.592E-05	49.942
3.0	2.0	2.5	3.0	2.0	3.0	3.5	4.0	1 505 569.90	2.156E-05	49.940
3.0	2.0	1.5	1.0	2.0	3.0	2.5	2.0	1 506 044.35	1.010E-05	49.933
3.0	2.0	1.5	2.0	2.0	3.0	2.5	3.0	1 506 147.85	1.575E-05	49.931
3.0	4.0	3.5		2.0	3.0	3.5		1 507 373.40	1.320E-04	49.942
3.0	4.0	3.5		2.0	3.0	2.5		1 507 632.30	3.586E-03	49.933
3.0	4.0	4.5		2.0	3.0	3.5		1 507 640.28	4.681E-03	49.942
3.0	4.0	3.5	3.0	2.0	3.0	2.5	3.0	1 507 689.50	1.457E-04	49.931
3.0	4.0	4.5	4.0	2.0	3.0	3.5	4.0	1 507 697.51	1.240E-04	49.940
3.0	3.0	2.5	2.0	2.0	2.0	1.5	1.0	1 511 748.46	1.787E-03	52.104
3.0	3.0	2.5	3.0	2.0	2.0	1.5	2.0	1 511 752.20	2.766E-03	52.104
3.0	3.0	2.5	2.0	2.0	2.0	1.5	2.0	1 511 761.91	2.116E-04	52.104
3.0	3.0	3.5	3.0	2.0	2.0	2.5	2.0	1 511 773.35	2.847E-03	52.102
3.0	3.0	3.5	4.0	2.0	2.0	2.5	3.0	1 511 777.08	3.830E-03	52.101
3.0	3.0	3.5	3.0	2.0	2.0	2.5	3.0	1 511 786.77	1.313E-04	52.101
3.0	3.0	2.5	3.0	2.0	2.0	2.5	2.0	1 511 817.37	1.314E-05	52.102
3.0	3.0	2.5	2.0	2.0	2.0	2.5	2.0	1 511 827.09	1.195E-04	52.102
3.0	3.0	2.5	3.0	2.0	2.0	2.5	3.0	1 511 830.79	1.999E-04	52.101
3.0	2.0	1.5	1.0	2.0	1.0	0.5	1.0	1 521 862.03	3.272E-04	49.406
3.0	2.0	2.5	2.0	2.0	1.0	1.5	2.0	1 521 884.33	2.203E-04	49.394
3.0	2.0	1.5	1.0	2.0	1.0	0.5	0.0	1 521 902.44	6.905E-04	49.404
3.0	2.0	1.5	2.0	2.0	1.0	0.5	1.0	1 521 907.76	1.744E-03	49.406
3.0	2.0	2.5	2.0	2.0	1.0	1.5	1.0	1 521 924.77	1.852E-03	49.393
3.0	2.0	2.5	3.0	2.0	1.0	1.5	2.0	1 521 930.08	2.901E-03	49.394
3.0	2.0	1.5	1.0	2.0	1.0	1.5	2.0	1 522 204.07	3.451E-05	49.394
3.0	2.0	1.5	1.0	2.0	1.0	1.5	1.0	1 522 244.52	1.906E-04	49.393
3.0	2.0	1.5	2.0	2.0	1.0	1.5	2.0	1 522 249.80	2.975E-04	49.394
3.0	2.0	1.5	2.0	2.0	1.0	1.5	1.0	1 522 290.24	2.949E-05	49.393
3.0	3.0	3.5	4.0	2.0	3.0	3.5	3.0	1 576 517.67	1.587E-05	49.942
3.0	3.0	3.5	3.0	2.0	3.0	3.5	3.0	1 576 527.36	4.027E-04	49.942
3.0	3.0	3.5	4.0	2.0	3.0	3.5	4.0	1 576 575.44	5.231E-04	49.940
3.0	3.0	2.5	2.0	2.0	3.0	3.5	3.0	1 576 581.09	1.569E-05	49.942
3.0	3.0	3.5	3.0	2.0	3.0	3.5	4.0	1 576 585.13	1.387E-05	49.940
3.0	3.0	2.5	3.0	2.0	3.0	3.5	4.0	1 576 629.15	2.101E-05	49.940
3.0	3.0	3.5	3.0	2.0	3.0	2.5	2.0	1 576 785.59	1.370E-05	49.933
3.0	3.0	2.5	3.0	2.0	3.0	2.5	2.0	1 576 829.61	2.075E-05	49.933
3.0	3.0	3.5	4.0	2.0	3.0	2.5	3.0	1 576 833.66	1.898E-05	49.931
3.0	3.0	2.5	2.0	2.0	3.0	2.5	2.0	1 576 839.32	2.758E-04	49.933
3.0	3.0	2.5	3.0	2.0	3.0	2.5	3.0	1 576 887.38	3.922E-04	49.931
3.0	3.0	2.5	2.0	2.0	3.0	2.5	3.0	1 576 897.09	1.878E-05	49.931
4.0	3.0	3.5	3.0	3.0	3.0	2.5	2.0	1 948 695.94	1.510E-05	102.531
4.0	3.0	3.5	3.0	3.0	3.0	3.5	3.0	1 948 749.67	3.952E-04	102.529
4.0	3.0	3.5	4.0	3.0	3.0	2.5	3.0	1 948 753.49	2.059E-05	102.531
4.0	3.0	3.5	3.0	3.0	3.0	3.5	4.0	1 948 759.36	1.531E-05	102.529
4.0	3.0	3.5	4.0	3.0	3.0	3.5	3.0	1 948 797.51	1.361E-05	102.529
4.0	3.0	3.5	4.0	3.0	3.0	3.5	4.0	1 948 807.20	5.139E-04	102.529
4.0	3.0	2.5	2.0	3.0	3.0	2.5	2.0	1 949 005.62	2.712E-04	102.531
4.0	3.0	2.5	2.0	3.0	3.0	2.5	3.0	1 949 015.33	2.041E-05	102.531
4.0	3.0	2.5	3.0	3.0	3.0	2.5	2.0	1 949 053.45	1.872E-05	102.531
4.0	3.0	2.5	2.0	3.0	3.0	3.5	3.0	1 949 059.36	1.346E-05	102.529
4.0	3.0	2.5	3.0	3.0	3.0	2.5	3.0	1 949 063.16	3.866E-04	102.531
4.0	3.0	2.5	3.0	3.0	3.0	3.5	4.0	1 949 116.87	1.895E-05	102.529
4.0	5.0	4.5		3.0	4.0	4.5		2 010 479.28	1.912E-04	100.231
4.0	5.0	4.5		3.0	4.0	3.5		2 010 745.53	8.458E-03	100.222
4.0	5.0	5.5		3.0	4.0	4.5		2 010 750.62	1.042E-02	100.231

Table 3 (cont).

N'	J'	F_1'	F'	N''	J''	F_1''	F''	ν [MHz][a,b]	A [s^{-1}]	E'' [cm^{-1}]
4.0	5.0	4.5	4.0	3.0	4.0	3.5	4.0	2 010 801.96	2.068E-04	100.220
4.0	5.0	5.5	5.0	3.0	4.0	4.5	5.0	2 010 807.06	1.814E-04	100.229
4.0	4.0	3.5	3.0	3.0	3.0	2.5	2.0	2 014 191.66	5.307E-03	102.531
4.0	4.0	3.5	4.0	3.0	3.0	2.5	3.0	2 014 193.74	7.150E-03	102.531
4.0	4.0	3.5	3.0	3.0	3.0	2.5	3.0	2 014 201.37	2.790E-04	102.531
4.0	4.0	4.5	4.0	3.0	3.0	3.5	3.0	2 014 205.11	7.236E-03	102.529
4.0	4.0	4.5	5.0	3.0	3.0	3.5	4.0	2 014 207.18	9.082E-03	102.529
4.0	4.0	4.5	4.0	3.0	3.0	3.5	4.0	2 014 214.81	1.943E-04	102.529
4.0	4.0	3.5	4.0	3.0	3.0	3.5	3.0	2 014 237.76	1.035E-05	102.529
4.0	4.0	3.5	3.0	3.0	3.0	3.5	3.0	2 014 245.39	1.856E-04	102.529
4.0	4.0	3.5	4.0	3.0	3.0	3.5	4.0	2 014 247.45	2.704E-04	102.529
4.0	3.0	3.5	3.0	3.0	4.0	4.5	4.0	2 017 637.30	1.223E-05	100.231
4.0	3.0	3.5	4.0	3.0	4.0	4.5	5.0	2 017 741.92	1.540E-05	100.229
4.0	3.0	2.5	3.0	3.0	4.0	3.5	4.0	2 018 317.82	1.220E-05	100.220
4.0	3.0	2.5	2.0	3.0	2.0	1.5	2.0	2 019 754.86	3.661E-04	100.171
4.0	3.0	3.5	3.0	3.0	2.0	2.5	3.0	2 019 764.90	2.850E-04	100.160
4.0	3.0	2.5	2.0	3.0	2.0	1.5	1.0	2 019 800.59	3.435E-03	100.169
4.0	3.0	2.5	3.0	3.0	2.0	1.5	2.0	2 019 802.69	5.359E-03	100.171
4.0	3.0	3.5	3.0	3.0	2.0	2.5	2.0	2 019 810.65	5.441E-03	100.159
4.0	3.0	3.5	4.0	3.0	2.0	2.5	3.0	2 019 812.74	7.361E-03	100.160
4.0	3.0	2.5	2.0	3.0	2.0	2.5	3.0	2 020 074.59	1.817E-05	100.160
4.0	3.0	2.5	2.0	3.0	2.0	2.5	2.0	2 020 120.34	2.699E-04	100.159
4.0	3.0	2.5	3.0	3.0	2.0	2.5	3.0	2 020 122.41	3.509E-04	100.160
4.0	3.0	2.5	3.0	3.0	2.0	2.5	2.0	2 020 168.16	1.461E-05	100.159
4.0	4.0	4.5	5.0	3.0	4.0	4.5	4.0	2 083 085.12	1.272E-05	100.231
4.0	4.0	4.5	4.0	3.0	4.0	4.5	4.0	2 083 092.74	5.356E-04	100.231
4.0	4.0	3.5	3.0	3.0	4.0	4.5	4.0	2 083 133.02	1.266E-05	100.231
4.0	4.0	4.5	5.0	3.0	4.0	4.5	5.0	2 083 141.90	6.577E-04	100.229
4.0	4.0	4.5	4.0	3.0	4.0	4.5	5.0	2 083 149.52	1.149E-05	100.229
4.0	4.0	3.5	4.0	3.0	4.0	4.5	5.0	2 083 182.17	1.591E-05	100.229
4.0	4.0	4.5	4.0	3.0	4.0	3.5	3.0	2 083 358.97	1.143E-05	100.222
4.0	4.0	3.5	4.0	3.0	4.0	3.5	3.0	2 083 391.62	1.582E-05	100.222
4.0	4.0	3.5	3.0	3.0	4.0	3.5	3.0	2 083 399.25	4.091E-04	100.222
4.0	4.0	4.5	5.0	3.0	4.0	3.5	4.0	2 083 408.13	1.466E-05	100.220
4.0	4.0	3.5	4.0	3.0	4.0	3.5	4.0	2 083 448.40	5.286E-04	100.220
4.0	4.0	3.5	3.0	3.0	4.0	3.5	4.0	2 083 456.03	1.460E-05	100.220
5.0	4.0	4.5	4.0	4.0	4.0	3.5	3.0	2 453 979.64	1.232E-05	169.717
5.0	4.0	4.5	4.0	4.0	4.0	4.5	4.0	2 454 019.92	5.267E-04	169.716
5.0	4.0	4.5	4.0	4.0	4.0	4.5	5.0	2 454 027.54	1.240E-05	169.715
5.0	4.0	4.5	5.0	4.0	4.0	3.5	4.0	2 454 036.21	1.566E-05	169.717
5.0	4.0	4.5	5.0	4.0	4.0	4.5	4.0	2 454 068.86	1.131E-05	169.716
5.0	4.0	4.5	5.0	4.0	4.0	4.5	5.0	2 454 076.48	6.482E-04	169.715
5.0	4.0	3.5	3.0	4.0	4.0	3.5	3.0	2 454 283.34	4.034E-04	169.717
5.0	4.0	3.5	3.0	4.0	4.0	3.5	4.0	2 454 290.98	1.561E-05	169.717
5.0	4.0	3.5	3.0	4.0	4.0	4.5	4.0	2 454 323.62	1.126E-05	169.716
5.0	4.0	3.5	4.0	4.0	4.0	3.5	3.0	2 454 332.27	1.452E-05	169.717
5.0	4.0	3.5	4.0	4.0	4.0	3.5	4.0	2 454 339.91	5.227E-04	169.717
5.0	4.0	3.5	4.0	4.0	4.0	4.5	5.0	2 454 380.18	1.461E-05	169.715
5.0	6.0	5.5		4.0	5.0	5.5		2 512 002.44	2.510E-04	167.303
5.0	6.0	5.5		4.0	5.0	4.5		2 512 273.77	1.639E-02	167.294
5.0	6.0	6.5		4.0	5.0	5.5		2 512 277.40	1.945E-02	167.303
5.0	6.0	5.5	5.0	4.0	5.0	4.5	5.0	2 512 329.71	2.677E-04	167.292
5.0	6.0	6.5	6.0	4.0	5.0	5.5	6.0	2 512 333.34	2.398E-04	167.301
5.0	5.0	4.5	4.0	4.0	4.0	3.5	3.0	2 515 353.26	1.153E-02	169.717
5.0	5.0	4.5	5.0	4.0	4.0	3.5	4.0	2 515 354.57	1.447E-02	169.717
5.0	5.0	4.5		4.0	4.0	3.5		2 515 361.85	7.452E-03	169.717
5.0	5.0	5.5	6.0	4.0	4.0	4.5	5.0	2 515 363.17	1.751E-02	169.715
5.0	5.0	5.5	5.0	4.0	4.0	4.5	5.0	2 515 369.49	2.561E-04	169.715
5.0	5.0	4.5	4.0	4.0	4.0	4.5	4.0	2 515 393.54	2.497E-04	169.716
5.0	5.0	4.5	5.0	4.0	4.0	4.5	5.0	2 515 394.84	3.369E-04	169.715
5.0	4.0	3.5	3.0	4.0	3.0	2.5	3.0	2 519 421.56	4.175E-04	167.544
5.0	4.0	4.5	4.0	4.0	3.0	3.5	4.0	2 519 427.52	3.476E-04	167.534
5.0	4.0	3.5	3.0	4.0	3.0	2.5	2.0	2 519 469.38	8.628E-03	167.543
5.0	4.0	3.5	4.0	4.0	3.0	2.5	3.0	2 519 470.49	1.166E-02	167.544
5.0	4.0	4.5	4.0	4.0	3.0	3.5	3.0	2 519 475.36	1.173E-02	167.532
5.0	4.0	4.5	5.0	4.0	3.0	3.5	4.0	2 519 476.47	1.476E-02	167.534
5.0	4.0	3.5	3.0	4.0	3.0	3.5	4.0	2 519 731.23	1.198E-05	167.534
5.0	4.0	3.5	3.0	4.0	3.0	3.5	3.0	2 519 779.07	3.374E-04	167.532

Table 3 (cont).

N'	J'	F_1'	F'	N''	J''	F_1''	F''	ν [MHz][a,b]	A [s^{-1}]	E'' [cm^{-1}]
5.0	4.0	3.5	4.0	4.0	3.0	3.5	4.0	2 519 780.16	4.072E-04	167.534
5.0	4.0	4.5	5.0	4.0	5.0	5.5	6.0	2 526 467.49	1.190E-05	167.301
5.0	5.0	5.5	6.0	4.0	5.0	5.5	5.0	2 587 698.01	1.058E-05	167.303
5.0	5.0	5.5	5.0	4.0	5.0	5.5	5.0	2 587 704.33	6.648E-04	167.303
5.0	5.0	4.5	4.0	4.0	5.0	5.5	5.0	2 587 736.00	1.056E-05	167.303
5.0	5.0	5.5	6.0	4.0	5.0	5.5	6.0	2 587 754.18	7.877E-04	167.301
5.0	5.0	4.5	5.0	4.0	5.0	5.5	6.0	2 587 785.85	1.276E-05	167.301
5.0	5.0	4.5	5.0	4.0	5.0	4.5	4.0	2 588 001.01	1.271E-05	167.294
5.0	5.0	4.5	4.0	4.0	5.0	4.5	4.0	2 588 007.33	5.388E-04	167.294
5.0	5.0	5.5	6.0	4.0	5.0	4.5	5.0	2 588 025.50	1.190E-05	167.292
5.0	5.0	4.5	5.0	4.0	5.0	4.5	5.0	2 588 057.17	6.596E-04	167.292
5.0	5.0	4.5	4.0	4.0	5.0	4.5	5.0	2 588 063.49	1.188E-05	167.292
6.0	5.0	5.5	5.0	5.0	5.0	4.5	4.0	2 956 982.94	1.033E-05	253.620
6.0	5.0	5.5	5.0	5.0	5.0	5.5	5.0	2 957 014.62	6.545E-04	253.619
6.0	5.0	5.5	5.0	5.0	5.0	5.5	6.0	2 957 020.93	1.036E-05	253.619
6.0	5.0	5.5	6.0	5.0	5.0	4.5	5.0	2 957 038.88	1.258E-05	253.620
6.0	5.0	5.5	6.0	5.0	5.0	5.5	6.0	2 957 070.55	7.773E-04	253.619
6.0	5.0	4.5	4.0	5.0	5.0	4.5	4.0	2 957 282.56	5.320E-04	253.620
6.0	5.0	4.5	4.0	5.0	5.0	4.5	5.0	2 957 288.88	1.257E-05	253.620
6.0	5.0	4.5	5.0	5.0	5.0	4.5	4.0	2 957 332.17	1.179E-05	253.620
6.0	5.0	4.5	5.0	5.0	5.0	4.5	5.0	2 957 338.49	6.531E-04	253.620
6.0	5.0	4.5	5.0	5.0	5.0	5.5	6.0	2 957 370.16	1.184E-05	253.619
6.0	7.0	6.5		5.0	6.0	6.5		3 011 789.72	3.106E-04	251.103
6.0	7.0	6.5		5.0	6.0	5.5		3 012 064.67	2.806E-02	251.094
6.0	7.0	7.5		5.0	6.0	6.5		3 012 067.45	3.247E-02	251.103
6.0	7.0	6.5	6.0	5.0	6.0	5.5	6.0	3 012 120.26	3.283E-04	251.092
6.0	7.0	7.5	7.0	5.0	6.0	6.5	7.0	3 012 123.04	2.985E-04	251.101
6.0	6.0	5.5	5.0	5.0	5.0	4.5	4.0	3 014 918.01	2.114E-02	253.620
6.0	6.0	6.5		5.0	5.0	5.5		3 014 924.09	2.553E-02	253.619
6.0	6.0	6.5	6.0	5.0	5.0	5.5	6.0	3 014 930.41	3.168E-04	253.619
6.0	6.0	5.5	5.0	5.0	5.0	5.5	5.0	3 014 949.69	3.122E-04	253.619
6.0	6.0	5.5	6.0	5.0	5.0	5.5	6.0	3 014 950.58	4.013E-04	253.619
6.0	5.0	4.5	4.0	5.0	4.0	3.5	4.0	3 018 303.55	4.724E-04	251.585
6.0	5.0	5.5	5.0	5.0	4.0	4.5	5.0	3 018 307.63	4.088E-04	251.575
6.0	5.0	4.5		5.0	4.0	3.5		3 018 352.86	1.917E-02	251.583
6.0	5.0	5.5		5.0	4.0	4.5		3 018 357.11	2.362E-02	251.573
6.0	6.0	6.5	6.0	5.0	6.0	6.5	6.0	3 090 351.25	7.912E-04	251.103
6.0	6.0	6.5	7.0	5.0	6.0	6.5	7.0	3 090 401.58	9.142E-04	251.101
6.0	6.0	5.5	6.0	5.0	6.0	6.5	7.0	3 090 427.17	1.062E-05	251.101
6.0	6.0	5.5	6.0	5.0	6.0	5.5	5.0	3 090 646.37	1.059E-05	251.094
6.0	6.0	5.5	5.0	5.0	6.0	5.5	5.0	3 090 651.79	6.658E-04	251.094
6.0	6.0	5.5	6.0	5.0	6.0	5.5	6.0	3 090 702.12	7.870E-04	251.092
7.0	6.0	6.5	6.0	6.0	6.0	6.5	6.0	3 457 722.42	7.794E-04	354.186
7.0	6.0	6.5	7.0	6.0	6.0	5.5	6.0	3 457 752.32	1.049E-05	354.187
7.0	6.0	6.5	7.0	6.0	6.0	6.5	7.0	3 457 777.91	9.029E-04	354.186
7.0	6.0	5.5	5.0	6.0	6.0	5.5	5.0	3 457 993.40	6.578E-04	354.187
7.0	6.0	5.5	5.0	6.0	6.0	5.5	6.0	3 457 998.82	1.048E-05	354.187
7.0	6.0	5.5	6.0	6.0	6.0	5.5	6.0	3 458 048.88	7.798E-04	354.187
7.0	8.0	7.5		6.0	7.0	7.5		3 509 589.74	3.699E-04	351.575
7.0	8.0	7.5		6.0	7.0	6.5		3 509 867.53	4.417E-02	351.566
7.0	8.0	8.5		6.0	7.0	7.5		3 509 869.70	5.015E-02	351.575
7.0	8.0	7.5	7.0	6.0	7.0	6.5	7.0	3 509 922.79	3.882E-04	351.564
7.0	8.0	8.5	8.0	6.0	7.0	7.5	8.0	3 509 925.03	3.571E-04	351.573
7.0	7.0	6.5		6.0	6.0	5.5		3 512 568.33	3.778E-02	354.187
7.0	7.0	7.5		6.0	6.0	6.5		3 512 573.16	4.374E-02	354.186
7.0	7.0	7.5	7.0	6.0	6.0	6.5	7.0	3 512 578.00	3.764E-04	354.186
7.0	7.0	6.5		6.0	6.0	6.5		3 512 593.93	1.188E-04	354.186
7.0	6.0	5.5	5.0	6.0	5.0	4.5	5.0	3 515 579.24	5.285E-04	352.266
7.0	6.0	6.5	6.0	6.0	5.0	5.5	6.0	3 515 582.28	4.690E-04	352.256
7.0	6.0	5.5		6.0	5.0	4.5		3 515 629.10	3.217E-02	352.265
7.0	6.0	6.5		6.0	5.0	5.5		3 515 632.14	3.819E-02	352.255
7.0	6.0	5.5		6.0	5.0	5.5		3 515 928.70	4.921E-04	352.255
7.0	7.0	7.5	7.0	6.0	7.0	7.5	7.0	3 590 856.54	9.153E-04	351.575
7.0	7.0	7.5	8.0	6.0	7.0	7.5	8.0	3 590 907.22	1.038E-03	351.573
7.0	7.0	6.5	6.0	6.0	7.0	6.5	6.0	3 591 155.27	7.903E-04	351.566
7.0	7.0	6.5	7.0	6.0	7.0	6.5	7.0	3 591 205.94	9.116E-04	351.564
8.0	7.0	7.5	7.0	7.0	7.0	7.5	7.0	3 955 966.12	9.018E-04	471.353
8.0	7.0	7.5	8.0	7.0	7.0	7.5	8.0	3 956 021.28	1.025E-03	471.353

Table 3 (cont).

N'	J'	F_1'	F'	N''	J''	F_1''	F''	ν [MHz][a,b]	A [s^{-1}]	E'' [cm^{-1}]
8.0	7.0	6.5	6.0	7.0	7.0	6.5	6.0	3 956 239.27	7.811E-04	471.354
8.0	7.0	6.5	7.0	7.0	7.0	6.5	7.0	3 956 294.43	9.035E-04	471.354
8.0	9.0	8.5		7.0	8.0	8.5		4 005 115.41	4.286E-04	468.652
8.0	9.0	8.5		7.0	8.0	7.5		4 005 395.39	6.534E-02	468.642
8.0	9.0	9.5		7.0	8.0	8.5		4 005 397.21	7.312E-02	468.652
8.0	9.0	8.5	8.0	7.0	8.0	7.5	8.0	4 005 450.48	4.474E-04	468.640
8.0	9.0	9.5	9.0	7.0	8.0	8.5	9.0	4 005 452.36	4.152E-04	468.650
8.0	8.0	7.5		7.0	7.0	6.5		4 007 984.85	5.711E-02	471.354
8.0	8.0	8.5		7.0	7.0	7.5		4 007 988.67	6.488E-02	471.353
8.0	8.0	8.5	8.0	7.0	7.0	7.5	8.0	4 007 993.00	4.348E-04	471.353
8.0	8.0	7.5		7.0	7.0	7.5		4 008 005.86	4.796E-04	471.353
8.0	7.0	6.5	6.0	7.0	6.0	5.5	6.0	4 010 763.80	5.847E-04	469.535
8.0	7.0	7.5	7.0	7.0	6.0	6.5	7.0	4 010 766.21	5.282E-04	469.525
8.0	7.0	6.5		7.0	6.0	5.5		4 010 814.03	4.978E-02	469.533
8.0	7.0	7.5		7.0	6.0	6.5		4 010 816.45	5.760E-02	469.523
8.0	7.0	6.5		7.0	6.0	6.5		4 011 110.67	5.505E-04	469.523
8.0	8.0	8.5	8.0	7.0	8.0	8.5	8.0	4 088 975.19	1.037E-03	468.652
8.0	8.0	8.5	9.0	7.0	8.0	8.5	9.0	4 089 026.14	1.159E-03	468.650
8.0	8.0	7.5	7.0	7.0	8.0	7.5	7.0	4 089 272.52	9.126E-04	468.642
8.0	8.0	7.5	8.0	7.0	8.0	7.5	8.0	4 089 323.46	1.034E-03	468.640
9.0	8.0	8.5	8.0	8.0	8.0	8.5	8.0	4 451 500.58	1.022E-03	605.045
9.0	8.0	8.5	9.0	8.0	8.0	8.5	9.0	4 451 555.48	1.145E-03	605.045
9.0	8.0	7.5	7.0	8.0	8.0	7.5	7.0	4 451 775.36	9.020E-04	605.046
9.0	8.0	7.5	8.0	8.0	8.0	7.5	8.0	4 451 830.27	1.024E-03	605.046
9.0	10.0	9.5		8.0	9.0	9.5		4 498 064.30	4.865E-04	602.257
9.0	10.0	9.5		8.0	9.0	8.5		4 498 346.15	9.219E-02	602.248
9.0	10.0	10.5	11.0	8.0	9.0	9.5	10.0	4 498 347.84	1.069E-01	602.255
9.0	10.0	9.5	9.0	8.0	9.0	8.5	9.0	4 498 401.15	5.057E-04	602.246
9.0	10.0	10.5	10.0	8.0	9.0	9.5	10.0	4 498 402.78	4.727E-04	602.255
9.0	9.0	8.5		8.0	8.0	7.5		4 500 849.01	7.707E-02	605.046
9.0	9.0	9.5	9.0	8.0	8.0	8.5	8.0	4 500 852.00	8.685E-02	605.045
9.0	9.0	9.5	9.0	8.0	8.0	8.5	9.0	4 500 856.29	4.919E-04	605.045
9.0	9.0	8.5		8.0	8.0	8.5		4 500 866.37	4.915E-04	605.045
9.0	8.0	7.5	7.0	8.0	7.0	6.5	7.0	4 503 470.30	6.407E-04	603.321
9.0	8.0	8.5	8.0	8.0	7.0	7.5	8.0	4 503 472.30	5.863E-04	603.312
9.0	8.0	7.5		8.0	7.0	6.5		4 503 520.68	6.776E-02	603.320
9.0	8.0	8.5		8.0	7.0	7.5		4 503 522.68	7.760E-02	603.310
9.0	8.0	7.5		8.0	7.0	7.5		4 503 814.83	5.807E-04	603.310
9.0	9.0	9.5	9.0	8.0	9.0	9.5	9.0	4 584 430.06	1.156E-03	602.257
9.0	9.0	9.5	10.0	8.0	9.0	9.5	10.0	4 584 481.22	1.278E-03	602.255
9.0	9.0	8.5	8.0	8.0	9.0	8.5	8.0	4 584 726.28	1.033E-03	602.248
9.0	9.0	8.5	9.0	8.0	9.0	8.5	9.0	4 584 777.43	1.153E-03	602.246
10.0	9.0	9.5	9.0	9.0	9.0	9.5	9.0	4 944 048.56	1.139E-03	755.177
10.0	9.0	9.5	10.0	9.0	9.0	9.5	10.0	4 944 103.26	1.262E-03	755.177
10.0	9.0	8.5	8.0	9.0	9.0	8.5	8.0	4 944 324.62	1.020E-03	755.178
10.0	9.0	8.5	9.0	9.0	9.0	8.5	9.0	4 944 379.32	1.143E-03	755.178
10.0	11.0	10.5		9.0	10.0	10.5		4 988 126.88	5.268E-04	752.306
10.0	11.0	10.5	11.0	9.0	10.0	9.5	10.0	4 988 410.46	1.313E-01	752.295
10.0	11.0	11.5	11.0	9.0	10.0	10.5	10.0	4 988 411.81	1.313E-01	752.306
10.0	11.0	10.5	10.0	9.0	10.0	9.5	10.0	4 988 465.30	5.630E-04	752.295
10.0	11.0	11.5	11.0	9.0	10.0	10.5	11.0	4 988 466.75	5.294E-04	752.304
10.0	10.0	9.5	9.0	9.0	9.0	8.5	8.0	4 990 842.33	1.068E-01	755.178
10.0	10.0	10.5		9.0	9.0	9.5		4 990 844.86	1.188E-01	755.177
10.0	10.0	9.5	9.0	9.0	9.0	8.5	9.0	4 990 846.24	6.458E-04	755.178
10.0	10.0	10.5	10.0	9.0	9.0	9.5	10.0	4 990 848.77	5.472E-04	755.177
10.0	10.0	9.5		9.0	9.0	9.5		4 990 856.70	5.482E-04	755.177
10.0	9.0	8.5	8.0	9.0	8.0	7.5	8.0	4 993 347.65	6.959E-04	753.543
10.0	9.0	9.5	9.0	9.0	8.0	8.5	9.0	4 993 349.36	6.434E-04	753.533
10.0	9.0	8.5		9.0	8.0	7.5		4 993 398.26	9.535E-02	753.541
10.0	9.0	9.5	9.0	9.0	8.0	8.5	8.0	4 993 399.98	1.074E-01	753.531
10.0	9.0	9.5	10.0	9.0	8.0	8.5	9.0	4 993 400.15	1.194E-01	753.533
10.0	9.0	8.5		9.0	8.0	8.5		4 993 690.41	6.379E-04	753.531
10.0	10.0	10.5	10.0	9.0	10.0	10.5	10.0	5 076 927.21	1.273E-03	752.306
10.0	10.0	10.5	11.0	9.0	10.0	10.5	11.0	5 076 978.54	1.394E-03	752.304
10.0	10.0	9.5	9.0	9.0	10.0	9.5	9.0	5 077 222.52	1.150E-03	752.297
10.0	10.0	9.5	10.0	9.0	10.0	9.5	10.0	5 077 273.85	1.270E-03	752.295
11.0	10.0	10.5	10.0	10.0	10.0	10.5	10.0	5 433 316.07	1.253E-03	921.654
11.0	10.0	10.5	11.0	10.0	10.0	10.5	11.0	5 433 370.61	1.377E-03	921.654

Table 3 (cont).

N'	J'	F_1'	F'	N''	J''	F_1''	F''	ν [MHz][a,b]	A [s^{-1}]	E'' [cm^{-1}]
11.0	10.0	9.5	9.0	10.0	10.0	9.5	9.0	5 433 593.16	1.136E-03	921.654
11.0	10.0	9.5	10.0	10.0	10.0	9.5	10.0	5 433 647.69	1.258E-03	921.654
11.0	12.0	11.5		10.0	11.0	11.5		5 474 989.85	5.825E-04	918.701
11.0	12.0	11.5		10.0	11.0	10.5		5 475 274.78	1.580E-01	918.692
11.0	12.0	12.5		10.0	11.0	11.5		5 475 276.09	1.725E-01	918.701
11.0	12.0	11.5	11.0	10.0	11.0	10.5	11.0	5 475 329.62	6.191E-04	918.690
11.0	12.0	12.5	12.0	10.0	11.0	11.5	12.0	5 475 330.93	5.852E-04	918.700
11.0	11.0	10.5		10.0	10.0	9.5		5 477 645.61	1.430E-01	921.654
11.0	11.0	11.5		10.0	10.0	10.5		5 477 647.80	1.575E-01	921.654
11.0	11.0	10.5	10.0	10.0	10.0	9.5	10.0	5 477 649.23	7.038E-04	921.654
11.0	11.0	11.5	11.0	10.0	10.0	10.5	11.0	5 477 651.42	6.004E-04	921.654
11.0	11.0	10.5		10.0	10.0	10.5		5 477 657.44	6.031E-04	921.654
11.0	10.0	9.5	9.0	10.0	9.0	8.5	9.0	5 480 060.08	7.503E-04	920.104
11.0	10.0	10.5	10.0	10.0	9.0	9.5	10.0	5 480 061.58	6.992E-04	920.095
11.0	10.0	9.5		10.0	9.0	8.5		5 480 110.86	1.292E-01	920.103
11.0	10.0	10.5		10.0	9.0	9.5		5 480 112.37	1.437E-01	920.093
11.0	10.0	9.5		10.0	9.0	9.5		5 480 401.30	6.938E-04	920.093
11.0	11.0	11.5	11.0	10.0	11.0	11.5	11.0	5 566 163.20	1.387E-03	918.701
11.0	11.0	11.5	12.0	10.0	11.0	11.5	12.0	5 566 214.68	1.508E-03	918.700
11.0	11.0	10.5	10.0	10.0	11.0	10.5	10.0	5 566 457.77	1.265E-03	918.692
11.0	11.0	10.5	11.0	10.0	11.0	10.5	11.0	5 566 509.24	1.384E-03	918.690
12.0	11.0	11.5	11.0	11.0	11.0	11.5	11.0	5 918 999.64	1.365E-03	104.369
12.0	11.0	11.5	12.0	11.0	11.0	11.5	12.0	5 919 054.04	1.488E-03	104.369
12.0	11.0	10.5	10.0	11.0	11.0	10.5	10.0	5 919 277.57	1.250E-03	104.369
12.0	11.0	10.5	11.0	11.0	11.0	10.5	11.0	5 919 331.97	1.371E-03	104.369
12.0	13.0	12.5		11.0	12.0	12.5		5 958 337.68	6.372E-04	101.337
12.0	13.0	12.5		11.0	12.0	11.5		5 958 623.92	2.039E-01	101.328
12.0	13.0	13.5		11.0	12.0	12.5		5 958 625.13	2.210E-01	101.337
12.0	13.0	12.5	12.0	11.0	12.0	11.5	12.0	5 958 678.69	6.741E-04	101.326
12.0	13.0	13.5	13.0	11.0	12.0	12.5	13.0	5 958 679.90	6.398E-04	101.335
12.0	12.0	11.5		11.0	11.0	10.5		5 960 939.88	1.863E-01	104.369
12.0	12.0	12.5		11.0	11.0	11.5		5 960 941.82	2.034E-01	104.369
12.0	12.0	11.5	11.0	11.0	11.0	10.5	11.0	5 960 943.26	7.615E-04	104.369
12.0	12.0	12.5	12.0	11.0	11.0	11.5	12.0	5 960 945.20	6.504E-04	104.369
12.0	12.0	11.5		11.0	11.0	11.5		5 960 949.52	6.557E-04	104.369
12.0	11.0	10.5	10.0	11.0	10.0	9.5	10.0	5 963 279.10	8.036E-04	102.901
12.0	11.0	11.5	11.0	11.0	10.0	10.5	11.0	5 963 280.45	7.538E-04	102.892
12.0	11.0	10.5		11.0	10.0	9.5		5 963 330.02	1.699E-01	102.900
12.0	11.0	11.5		11.0	10.0	10.5		5 963 331.38	1.871E-01	102.890
12.0	11.0	10.5		11.0	10.0	10.5		5 963 618.95	7.483E-04	102.890

and lower states of the transitions excepts for those transitions which cannot be resolved, for which the F quantum number is unlisted. The uncertainties for the frequency predictions were calculated proportionally to the inverse square of the uncertainties of the molecular constants quoted in Table 2 and are less than 1 MHz.

IV. Interstellar Phosphorus Chemistry

The ion-molecule chemistry of phosphorus species in the gas phase of dense interstellar clouds starts from the atomic ion P^+, which can react with a variety of moderately abundant gaseous species such as H_2O, O_2, CO_2, and NH_3 [21, 22] to form ions such as HPO^+, PO^+, H_2PN^+. These ionic species then produce neutral molecules via dissociative recombination reactions with electrons [23]. Although the processes have not yet been studied in the laboratory, it is likely that PH is produced via a number of dissociative recombination reactions involving HPO^+, H_2PN^+, and other ions [24]. Once produced, PH is probably destroyed most rapidly via neutral-neutral reactions such as [25]

$$PH + N \longrightarrow PN + H. \qquad (2)$$

According to the latest model results [25], the fractional abundance of PH compared with the gas density is $\approx 10^{-11}$, which, although low compared with most detected interstellar molecules, is large enough for detection given precisely known frequencies and dedicated observing runs. A complication arises from the fact that PN, an observed interstellar molecule with a fractional abundance of $\approx 10^{-11} - 10^{-10}$ [13, 26], is detected in regions of relatively high excitation near newly formed and forming stars rather than in the ambient low temperature interstellar medium. This may imply that high temperatures are needed for sufficient amounts of the element phosphorus to be driven off the surfaces of interstellar dust particles into the gas phase so as to initiate the reaction sequences discussed above.

Acknowledgements

The work in Köln was supported in part by the Deutsche Forschungsgesellschaft (DFG) via grant SFB 301 and special funding from the Science Ministry of the Land Nordrhein-Westfalen. E. H. wishes to acknowledge the support of NASA for work at Ohio State in laboratory astrophysics.

[1] G. Winnewisser, Vib. Spectrosc. **8**, 241 (1995).
[2] F. Hund, Z. Physik **36**, 657 (1926).
[3] E. Klisch, Th. Klaus, S. P. Belov, G. Winnewisser, and E. Herbst, in "Amazing Light", ed. R. Y. Chiao, Springer-Verlag, New York 1996, pp. 355.
[4] E. Klisch, Th. Klaus, S. P. Belov, A. Dolgner, R. Schieder, and G. Winnewisser, Astrophys. J. **473**, 1118 (1996).
[5] Th. Klaus, S. Takano, and G. Winnewisser, Astronom. Astrophys. **322**, L1 (1997).

[6] S. Takano, Th. Klaus, and G. Winnewisser, J. Mol. Spectrosc. 1998, in press.
[7] F. Legay, Can. J. Phys. **38**, 797 (1960).
[8] J. Rostas, D. Cossart, and J. R. Bastien, Can. J. Phys. **52**, 1274 (1974).
[9] P. B. Davies, D. K. Runel, and B. A. Trush, Chem. Phys. Lett. **36**, 280 (1975).
[10] H. Uehara and K. Hakuta, J. Chem. Phys. **74**, 4326 (1981).
[11] N. Ohashi, K. Kawaguchi, and E. Hirota, J. Mol. Spectrosc. **103**, 337 (1984).
[12] M. Goto and S. Saito, Chem. Phys. Lett. **211**, 443 (1993).
[13] B. E. Turner and J. Bally, Astrophys. J. **321**, L75 (1987).
[14] M. Guélin, J. Cernicharo, G. Paubert, and B. E. Turner, Astron. Astrophys. **230**, L9 (1990).
[15] S. P. Belov, F. Lewen, Th. Klaus, and G. Winnewisser, J. Mol. Spectrosc. **174**, 606 (1995).
[16] C. H. Townes and A. L. Schawlow, "Microwave Spectroscopy", Dover Publications, Inc., New York 1975.
[17] International Union of Pure and Applied Chemistry, IUPAC, "Quantities, Units, and Symbols" in Physical Chemistry, Alden Press, Oxford 1988.
[18] R. A. Frosch and H. M. Foley, Phys. Rev. **88**, 1337 (1952).
[19] E. Klisch, Th. Klaus, S. P. Belov, G. Winnewisser, and E. Herbst, Astron. Astrophys. **304**, L5 (1995).
[20] M. J. Frisch, G. W. Trucks, H. B. Schlegel, P. M. W. Gill, B. G. Johnson *et al.*, Gaussian 94, Revision E2, Inc., Pittsburgh (PA) 1995.
[21] L. R. Thorne, V. G. Anicich, S. S. Prasad, and W. T. Huntress, Jr., Astrophys. J. **280**, 139 (1984).
[22] D. Smith, B. J. McIntosh, and N. G. Adams, J. Chem. Phys. **90**, 6213 (1989).
[23] M. Larsson, Annu. Rev. Phys. Chem. **48**, 151 (1997).
[24] T. J. Millar, A. Bennett, and E. Herbst, Mon. Not. R. Astr. Soc. **229**, 41P (1987).
[25] H.-H. Lee, R. P. A. Bettens, and E. Herbst, Astron. Astrophys. Suppl. Ser. **119**, 111 (1996).
[26] L. M. Ziurys, Astrophys. J. **321**, L81 (1987).